

Sensitive CO(1-0) Survey in Pegasus-Pisces Reduces CO-Dark Gas Inventory by Factor of Two

Emmanuel Donate¹ * and Loris Magnani¹

¹*Department of Physics and Astronomy, University of Georgia, Athens, GA 30602, USA*

28 September 2018

ABSTRACT

We conducted high-sensitivity, high-velocity resolution CO(1-0) observations in a region containing a portion of the diffuse molecular cloud MBM 53 to determine whether weak CO emission was present. The results of our observations increase the amount of CO-detectable molecular gas in the region by a factor of two. The increased molecular mass for the cloud, if applicable to the molecular clouds in the entire Pegasus-Pisces region, decreases the dark molecular gas content from 58% of the total H₂ mass to $\sim 30\%$. If the results for MBM53 are applicable to other diffuse clouds, then the fraction of dark gas directly detectable via sensitive CO(1-0) observations in diffuse molecular clouds is similar to that predicted by models for Giant Molecular Clouds.

Key words: ISM: clouds – ISM: molecules.

1 INTRODUCTION

The idea that substantial molecular gas is present in the interstellar medium (ISM) but is not detectable by the CO(1-0) emission line has become fairly prevalent in the last decade. This component has become known as “dark gas”, a term first suggested in a paper describing its properties and extent by Grenier, Casandjian and Terrier (2005; hereafter GCT)¹. GCT used a combination of gamma-ray and infrared data to identify regions with cold dust. By comparing these with maps of CO and HI emission, they found that a significant fraction of the H₂ mass is not traced by the CO(1-0) observations. Their main conclusion is that the dark gas mass in the Milky Way is comparable to the molecular mass detected by CO(1-0) emission. More recent studies corroborate this (Abdo et al. 2010; Planck Collaboration, Planck Early Results, 2011, Paper XIX).

This phenomenon is predicted by models of photo-dissociation regions (PDRs) (e.g., Hollenbach & Tielens 1997). The depths into a PDR at which H₂ and CO form depend directly on the intensity of the interstellar radiation field and the volume density of hydrogen nucleons. It is convenient from the observational point of view to talk about depth into a PDR in terms of extinction or color excess. Liszt (2014) ascribes a break in slope in the N(HI) - E(B-V)

relation at $E(B-V) \sim 0.1$ mag to the onset of H₂ formation. For a standard interstellar radiation field (e.g., Draine 1978), the models of van Dishoeck & Black (1988) show a significant rise in both N(CO) and the CO/H₂ ratio at $N(\text{H}_2) \sim 1 \times 10^{21} \text{ cm}^{-2}$, equivalent to $E(B-V) \approx 0.3$ mag or $A_V \approx 1$ mag. Thus, under normal conditions, CO-dark gas should be found in regions with $0.1 \lesssim E(B-V) \lesssim 0.3$ mag.

van Dishoeck & Black defined *diffuse* molecular clouds as those with $A_V \leq 1$ mag. Before the development of sensitive millimeter-wave receivers, observations of diffuse molecular clouds were confined to optical and UV absorption lines. However, under certain conditions, CO(1-0) emission can trace diffuse molecular gas fairly easily (e.g., Liszt, Pety, and Lucas 2010), complicating the picture described above. But even by the late 1980s, CO(1-0) detections in regions with $A_V < 1$ mag were possible. For instance, many of the high-latitude clouds identified by Magnani, Blitz, and Mundy (1985) have $A_V < 1$ mag and yet are readily detectable by CO(1-0) emission. More recently, Chastain et al. (2006), Liszt and Pety (2012), and Cotten and Magnani (2013) detected CO(1-0) lines from regions with $E(B-V)$ as low as 0.1 mag. Clearly, under certain conditions to be explained, CO(1-0) emission can trace gas in the dark molecular regime.

One of the fields studied by GCT includes 1888 square degrees centered on Pegasus-Pisces for which they obtain the ratios of CO-detectable molecular gas, to CO-dark gas, to atomic gas. We will abbreviate these ratios as H₂:DG:HI. The CO-detectable molecular gas was determined from estimates of the masses of some of the mapped high-latitude

* E-mail: edonate@uga.edu (ED)

¹ Some of the dark gas may be in atomic form and not readily detectable by the 21 cm line because of opacity effects. In this paper we will focus on the *molecular* dark gas.

clouds in the region, and GCT derive $\text{H}_2:\text{DG}:\text{HI}$ to be 0.7: 1.0: 3.4, with a total mass of $1.6 \times 10^4 M_\odot$. However, of the many molecular clouds in the region, GCT only included the MBM 53-55 complex and its environs as mapped by Yamamoto et al. (2003 - hereafter Y2003; 2006). Blair et al. (2017) examine the Magnani et al. (2000) high-latitude CO(1-0) survey and, by including all known molecular clouds in the region, revise the $\text{H}_2:\text{DG}:\text{HI}$ ratios to 0.9: 1.0: 3.8. Even with this revision, the CO-dark gas fraction is still significant. But are the dark gas regions described by GCT really undetectable in CO(1-0)? A key factor is the sensitivity of the CO(1-0) observations. While the total mass in hydrogen nucleons for Pegasus-Pisces derived by GCT may be correct, the breakdown into $\text{H}_2:\text{DG}:\text{HI}$ depends on the sensitivity of the CO observations of the molecular clouds in the region. If more sensitive observations of these clouds were available, the CO-detectable molecular mass might increase at the expense of the CO-dark gas fraction.

In this paper we examine whether sensitive CO(1-0) observations can reveal the presence of at least some of the dark gas in a high-latitude region containing a portion of a diffuse molecular cloud (MBM 53). In section 2, we discuss the Magnani et al. (2000) Southern Galactic Hemisphere high-latitude CO(1-0) survey (SGH-HL) and the region in Pegasus-Pisces that overlaps one of the GCT fields. We describe the observational set-up in section 3 and, in section 4, we compare our results with those from GCT. We then estimate the fraction of dark gas detectable by very sensitive CO(1-0) observations. A discussion and summary is presented in section 5.

2 THE SGH HIGH-LATITUDE SURVEY IN PEGASUS-PISCES

GCT derived their quantitative conclusions on the dark gas by examining seven nearby areas, one of which substantially overlaps a portion of the SGH-HL survey (see Figure 1). The area called Pegasus by GCT and Pegasus-Pisces in this paper is bounded by the black box. Of the 4982 grid points observed in the SGH by Magnani et al. (2000), 2080 points are located within the region that overlaps 84% of the GCT Pegasus field². In that region, Magnani et al. (2000) recorded 48 CO detections with an rms in T_{mb} of 0.1 K for a detection rate of 0.023.

GCT quote values for the molecular mass in the Pegasus-Pisces region in CO-detectable H_2 and CO-dark H_2 of $2200 M_\odot$ and $3100 M_\odot$, respectively. Their estimate of the CO-detectable H_2 in the region comes solely from the MBM 53-55 cloud complex as mapped by Y2003. We presume that the difference in the molecular mass estimate of the complex between GCT and the Y2003 value is due to GCT using a value of $X_{CO}^3 = 1.74 \times 10^{20} \text{ cm}^{-2} [\text{K km s}^{-1}]^{-1}$ rather than the value of $1.0 \times 10^{20} \text{ cm}^{-2} [\text{K km s}^{-1}]^{-1}$ used by Y2003. Despite the presence of other clouds in the region (see Blair et al. 2017), we assume, for the moment, that the

² The GCT Pegasus region extends over $-60^\circ \leq b \leq -26^\circ$, but the SGH-HL CO survey begins at $b = -30^\circ$.

³ X_{CO} is the empirically derived conversion factor between $N(\text{H}_2)$ and the velocity-integrated CO(1-0) main beam antenna temperature.

total mass in hydrogen nucleons detected by GCT is accurate, hence any increase in the CO-detected gas in the MBM 53-55 clouds must come at the expense of the dark gas mass.

As mentioned above, the key factor in determining the amount of CO-detected gas is the sensitivity of the CO(1-0) observations. More sensitive (lower rms) CO observations should yield new detections of molecular gas at cloud edges. For example, the high-latitude cloud MBM 40 was sampled over 103 lines of sight in the CO(1-0) line at sensitivities of 0.05 - 0.11 K (1σ rms in T_R^* , or 0.06 - 0.13 K in T_{mb}) by Cotten & Magnani (2013). Sampling was over the whole cloud, including the outermost parts of the cloud with $E(\text{B-V}) \lesssim 0.12$ mag. There, weak CO emission was present in 13 out of 21 lines of sight. The antenna temperature, T_R^* , ranged from 0.11 - 2.29 K for the 13 detections with 7 of those ranging from 0.11 - 0.61 K. Many of these latter detections would have been missed by conventional mapping which typically has rms antenna temperature of a few tenths of a K. By including the molecular mass detected by the sensitive CO observations of the outermost region of MBM 40, the cloud mass estimate increased from $20 M_\odot$ (Chastain 2007) to $32 M_\odot$.

To determine how much molecular gas could be detected by a more sensitive CO survey at high Galactic latitude, we re-observed a small region of the SGH-HL survey in Pegasus-Pisces. The SGH-HL survey has 2080 observed lines of sight within the black box in Figure 1 with $T_{mb} \approx 0.1$ K for the 1σ rms value. Since our goal was to improve this by at least a factor of 4-5, we had to choose a significantly smaller region to sample. We wanted an area containing at least a portion of a known molecular cloud (because GCT emphasized that dark gas regions “...surround all the nearby CO clouds and bridge the dense cores to broader atomic clouds...”). Moreover, the only cloud complex recognized by GCT in the Pegasus-Pisces region in Figure 1 is MBM 53-55, thus, by choosing a region containing at least part of this complex, we can directly compare how our mass estimates for a portion of this complex change with more sensitive observations. We settled on the region bounded by $80.3^\circ \leq \ell \leq 99.0^\circ$; $-34^\circ \leq b \leq -30.0^\circ$. This area includes five detections of MBM 53 from the SGH-HL survey. The location of the 88 points we observed is shown in Figure 2. The five CO(1-0) detections from the SGH-HL survey arising from the diffuse high-latitude cloud MBM 53 are noted in the figure.

3 OBSERVATIONS

The CO(1-0) observations were made at the 12 m mm-wave telescope of the Arizona Radio Observatory on Kitt Peak. We used the 3 mm ALMA Type Band 3 dual-polarization receiver with system temperatures on the sky typically less than 200 K (single sideband). The antenna temperature scale, T_A^* (see Kutner and Ulich 1981), is set by the chopper wheel method and is given at the telescope as T_R^* , the antenna temperature corrected for spillover and scattering. Conversion to the main beam brightness temperature, T_{mb} is via T_R^*/η_{mb} , where η_{mb} is the main beam efficiency (at 115 GHz, $\eta_{mb} \approx 0.85$). We assume that the source fills the beam so that the beam filling factor is unity. The backend spectrometers were the Millimeter Autocorrelator (MAC) and the 250 kHz filter banks. The MAC was configured to

have 200 MHz total bandwidth (150 MHz of usable bandwidth) over 6144 channels for a frequency resolution of 24.4 kHz per channel equivalent to 0.063 km s^{-1} . The 250 kHz filter banks were used as a backup for the MAC and have a velocity resolution per channel of 0.65 km s^{-1} . A fiducial position ($\ell = 92.4^\circ; b = -34.0^\circ$) with a strong CO line was monitored each day and a Gaussian fit to the line showed variations in peak T_R^* of less than 5% in clear weather.

The observations were made in on-off mode with an absolute off-position with the lowest reddening in the region $[E(B-V) = 0.03 \text{ mag at (R.A., Dec) = (22^h 37^m 37.6^s; 23^\circ 35' 20.2'')]$ as given by the Schlegel, Finkbeiner, and Davis (1999) dust maps. At 115 GHz, the beam size of the 12-m telescope is $55''$. The SGH-HL survey was sampled every degree in Galactic longitude and latitude at a resolution of $8.4'$ for an under sampling of a factor of ~ 60 . A meaningful comparison between the CO observations from the two telescopes requires that we “map” the $8.4'$ beam with our ARO 12-m telescope observations. We thus sampled each of the 88 points in Figure 2 using the thirteen-point pattern shown in Figure 3. Although the areal ratio is approximately 0.155, the thirteen point sampling pattern was the best compromise between covering the $8.4'$ beam from the SGH-HL survey and achieving the factor of 5 improvement in sensitivity we desired. There could be even more CO emission in the region if isolated, small-scale structures exist in the periphery of the cloud. This issue will be addressed in a separate paper.

A comparison of the integrated antenna temperature for the five detected positions from SGH-HL with our thirteen-point pattern averaged to form a single spectrum for each position shows very good agreement (see Table 1 and discussion in §3.1). With two minutes on source and two minutes off, each summed spectrum consisted of 26 minutes on-source resulting in rms values per channel for the MAC of 11 - 45 mK.

The results of our observations are shown in Table 2. Fifteen new detections were made for a total of 20 out of 88 observed lines of sight detectable in the CO(1-0) line. Figure 2 shows the distribution of the new and previously known detections. Representative spectra of some of the new detections are shown in Figure 4a-c.

3.1 Comparison with earlier results

Five of the ARO detections had been previously detected with the Harvard-Smithsonian Center for Astrophysics 1.2 m telescope (Magnani et al. 2000). As can be seen from Table 1, the agreement between the two sets of observations is quite good. The SGH-HL observations were about a factor of five less sensitive in T_{mb} while the difference in W_{CO} 1σ uncertainties improves for the ARO observations by factors of about 2 to 6. For the ARO data, W_{CO} is calculated from the parameters of the Gaussian fit as $1.07[T_{mb}\Delta v(\text{FWHM})]$. The total W_{CO} for the five SGH-HL detections is $7.56 \pm 0.93 \text{ K km s}^{-1}$ and, for the ARO observations, $8.53 \pm 0.37 \text{ K km s}^{-1}$, so that estimates of the mass based on these results would be consistent. However, because of the limited sampling of the SGH-HL beam by our current observations we note that the ARO results are lower limits.

When looking at Table 2, some of the new ARO detections have W_{CO} values that should have been detected by

the SGH-HL survey. An example of this is position G902-33, with $T_R^* \approx 0.4 \text{ K}$, equivalent to $T_{mb} \approx 0.5 \text{ K}$. The rms sensitivity of the SGH-HL survey was 0.1 K and should have resulted in a detection. However, the SGH-HL spectrum shown in top half of Figure 5 shows no evidence of the line. This issue can be understood by noting the narrowness of the line at this position (0.6 km s^{-1}) compared to the velocity resolution of the filter banks used in the SGH-HL survey: 0.65 km s^{-1} . The line, if it had been detected would have been in only 1-2 channels, making it more susceptible to noise fluctuations than if higher frequency resolution was employed. Figure 5 shows the non-detection from SGH-HL compared to the spectrum from the data presented in this paper. The surprise here is the importance of observing diffuse molecular cloud at high velocity resolution.

3.2 The mass of MBM 53-55

Since we are re-observing a part of the MBM 53-55 region sampled in CO(1-0) by Magnani et al. (2000), any new detections will increase the mass of that cloud complex. Here we determine the mass of the complex from the original Magnani et al. (2000) data and compare our result to that of Y2003. The Pegasus-Pisces region (with northernmost boundary $b = -30^\circ$) shown in Figure 1 covers 0.5749 steradians. The SGH-HL survey covers this region with 2080 points. Of the 48 detections in this region, 23 are associated with the MBM 53-55 cloud complex (see Magnani et al. 2000) providing an estimate of the solid angle of the cloud. We can derive the mass of these clouds using the average W_{CO} value from SGH-HL (2.47 K km s^{-1}), the distance to the clouds (150 pc), a value for the mean molecular weight of 2.8, and $X_{CO} = 1.0 \times 10^{20} \text{ cm}^{-2} [\text{K km s}^{-1}]^{-1}$. The latter three values were chosen to be identical to those used by Y2003. In this fashion we obtain a mass of $790 M_\odot$ compared to $1200 M_\odot$ by Y2003. In comparing these results, we note that the region surveyed by Y2003 is slightly larger than ours, extending to $b = -29^\circ$, but the clouds there are not very prominent and contribute little mass to the complex. The discrepancy in the mass estimate is also not due to sensitivity considerations since the SGH-HL survey has an rms of 0.1 K versus 0.5 for Y2003. The reasons are likely to be either the peculiar sampling method used by Magnani et al. (2000) where the off position for the spectra was chosen to be one degree south of the on scan (see discussion by Hartmann, Magnani, and Thaddeus 1998), beam dilution of small structures at the cloud edges, and/or non-detections of narrow lines because of the relatively poor velocity resolution of the SGH-HL survey (see discussion above). The SGH-HL survey has a beam of $8.4'$ and a velocity resolution of 0.65 km s^{-1} versus $2.6'$ and 0.1 km s^{-1} , respectively, for Y2003.

GCT increase the Y2003 mass estimate to $2200 M_\odot$ by using a larger value of X_{CO} . If we increase the SGH-HL result by the same factor, the mass of the clouds would then be $1450 M_\odot$. This is the result we will use for the CO-detected mass in the MBM 53-55 complex based on the SGH-HL survey.

Table 1. W_{CO} for the five positions in common between the SGH-HL and the current survey.

Position	ℓ deg	b deg	W_{CO}^a (SGH-HL) K km s ⁻¹	W_{CO}^a (this paper) K km s ⁻¹
G92.4–34	92.4	–34.0	4.09±0.39	4.41±0.19
G93.5–32	93.5	–32.0	0.57±0.39	0.50±0.06
G94.6–34	94.6	–34.0	1.44±0.40	1.49±0.24
G96.8–30	96.8	–30.0	0.46±0.50	0.86±0.10
G99.0–31	99.0	–31.0	1.00±0.39	1.27±0.18
Total	—	—	7.56±0.93	8.53±0.37

^a W_{CO} is defined as $\int T_{mb} dv$

Table 2. Gaussian-fit parameters and W_{CO} for CO(1-0) detections in our survey.

Position	ℓ deg	b deg	T_R^* K	Δv km s ⁻¹	v_{LSR} km s ⁻¹	W_{CO}^a K km s ⁻¹	Notes
G92.4–30	92.4	–30.0	0.14±0.04	1.85	–9.99	0.33±0.13	redshifted and blueshifted wings on profile ^c
G93.5–30	93.5	–30.0	0.36±0.04	2.12	–10.09	0.96±0.15	
G96.8–30	96.8	–30.0	0.62±0.05	1.10	–14.90	0.86±0.10	
G92.4–31	92.4	–31.0	0.35±0.09 ^b	1.25	–14.66	0.46±0.50	Magnani et al. (2000)
			0.25±0.03	1.11	–5.44	0.35±0.06	first component ^d
G93.5–31	93.5	–31.0	0.14±0.03	0.73	–8.32	0.13±0.04	second component
			0.65±0.05	0.92	–3.15	0.75±0.08	first component
G97.9–31	97.9	–31.0	0.43±0.05	0.95	–4.72	0.51±0.08	second component
			0.097±0.033	0.88	–11.61	0.11±0.05	
G99.0–31	99.0	–31.0	0.49±0.05	2.06	–8.18	1.27±0.18	blueshifted wing on profile
			0.27±0.07 ^b	3.41	–8.47	1.00±0.39	Magnani et al. (2000)
G92.4–32	92.4	–32.0	0.23±0.03	1.01	–2.33	0.29±0.05	first component - redshifted wing on profile
			0.11±0.03	0.91	–7.86	0.13±0.05	second component
G93.5–32	93.5	–32.0	0.43±0.03	0.63	–4.67	0.34±0.03	first component
			0.14±0.03	0.89	–3.95	0.16±0.05	second component
G94.6–32	94.6	–32.0	0.37±0.07 ^b	1.46	–4.60	0.57±0.39	Magnani et al. (2000)
			0.48±0.03	0.71	–2.91	0.43±0.04	
G95.7–32	95.7	–32.0	0.32±0.03	2.86	–6.40	1.15±0.15	
G99.0–32	99.0	–32.0	0.31±0.03	1.13	–6.71	0.44±0.06	
G90.2–33	90.2	–33.0	0.38±0.03	0.60	–0.56	0.28±0.03	
G92.4–33	92.4	–33.0	0.076±0.028	2.05	–5.22	0.20±0.10	first component
			0.077±0.028	1.20	–8.63	0.12±0.06	second component
G97.9–33	97.9	–33.0	0.31±0.04	0.98	–1.62	0.38±0.07	first component
			0.10±0.04	1.36	–3.58	0.17±0.09	second component
G92.4–34	92.4	–34.0	1.52±0.05	2.01	–7.48	3.85±0.18	first component
			0.54±0.05	0.83	–7.27	0.56±0.07	second component
G93.5–34	93.5	–34.0	1.34±0.07 ^b	2.84	–7.47	4.09±0.39	Magnani et al. (2000)
			0.61±0.03	1.46	–4.21	1.12±0.08	blueshifted wing centered at ~ -7 km s ⁻¹
G94.6–34	94.6	–34.0	0.51±0.06	1.81	–6.06	1.17±0.19	first component
			0.20±0.06	1.27	–2.92	0.32±0.14	second component
G95.7–34	95.7	–34.0	0.49±0.07 ^b	2.77	–6.13	1.44±0.40	Magnani et al. (2000)
			0.31±0.04	0.69	–4.89	0.27±0.05	
G96.8–34	96.8	–34.0	0.37±0.04	2.88	–12.58	1.34±0.21	first component
			0.21±0.04	1.66	–7.07	0.44±0.12	second component
							redshifted wing centered at ~ -4.5 km s ⁻¹

^a W_{CO} is defined as $\int T_{mb} dv$

^b T_{mb} from Magnani et al. (2000)

^c Some of the line profiles were not well-fit by one or two Gaussians and showed weak emission in either the blue or red (or both) wings of the profile. In these instances, the quoted value of W_{CO} is an underestimate since it is estimated based on the Gaussian fits.

^d Some of the line profiles showed two distinct components.

4 RESULTS AND IMPLICATIONS

The 15 new detections from our ARO observations more than double the W_{CO} value from the SGH-HL survey (from 8.53 K km s^{-1} to $18.42 \text{ K km s}^{-1}$, see Tables 2 and 3). Since the cloud mass is directly proportional to W_{CO} , if our results are typical for the rest of the cloud complex, then the overall mass would increase by a factor of 2.16. Given the results of §3.2, this would mean that the mass of the MBM 53-55 complex would increase on the basis of our sensitive, high velocity resolution CO observations from $1450 M_{\odot}$ to $3130 M_{\odot}$.

GCT derive $\text{H}_2:\text{DG}:\text{HI}$ for the entire Pegasus-Pisces region to be 0.7: 1.0: 3.4. If the total mass from the gamma-ray data is $1.6 \times 10^4 M_{\odot}$, then the ratio $\text{H}_2:\text{DG}:\text{HI}$ in solar masses would be 2200: 3100: 10,700 M_{\odot} . Assuming the atomic hydrogen is well-determined (i.e., there are no opacity issues), the increase of $930 M_{\odot}$ in CO-detectable gas (i.e., from GCT's value of $2200 M_{\odot}$ to our value of $3130 M_{\odot}$) must come at the expense of the CO-dark gas. This would reduce the CO-dark gas in the region from GCT's estimate of $3100 M_{\odot}$ to $2170 M_{\odot}$. The total molecular gas content (i.e., CO-detectable plus dark) remains the same, so the CO-dark gas contribution to the total molecular gas now decreases to about $\sim 40\%$.

These results are based on sampling 88 of the 2080 points observed in the SGH-HL survey for this region. Our observations focus on the northernmost portion of the MBM 53-55 complex which is the only molecular gas considered by GCT in the region. The locations of our new detections (see Figure 2) are, for the most part, in the outer regions of the cloud, where low-intensity CO-emitting gas should be located. Since the region chosen for our high-sensitivity observations was chosen randomly along the MBM 53-55 cloud, it seems reasonable to assume that this pattern holds throughout the cloud. A similar result was obtained for the diffuse molecular cloud, MBM 40, by Cotten & Magnani (2013) who derived a mass of $32 M_{\odot}$ from sensitive CO(1-0) observations (rms values 0.05 - 0.09 K). Conventional CO maps of this cloud (i.e., with rms values of 0.1 - 0.7 K in antenna temperature) yielded mass estimates in the 11-20 M_{\odot} range (Magnani, Hartmann, & Speck 1996; Chastain 2005).

If our results are applicable to other regions, then \sim one-third of the CO-dark gas is not “dark” as far as CO observations are concerned. Unfortunately, the long integration times necessary to detect much of the low-level CO emission reported in this paper, likely preclude any significant mapping of this portion of the dark gas.

The best spectroscopic tracer of dark gas is the [CII] line at $158 \mu\text{m}$ since the integration times are more reasonable (e.g., Langer et al. 2010; Langer et al. 2014). The other spectroscopic candidates for tracing dark gas are the OH 18 cm main lines and, in particular, the 1667 MHz line. Several studies [Barriault et al, 2010; Cotten et al. (2012); and Allen et al. (2015)] have indicated that OH observations may pick up molecular gas not detectable in CO - but these authors compared their results to conventional CO mapping with rms values $\sim 0.1 \text{ K}$. We believe that sensitive CO(1-0) observations like the ones reported here would be as successful in detecting a portion of the dark gas as OH, and with comparable integration times.

Our results are based on the assumption that the low-

level emission we detected during our survey can be analyzed in the same manner as the stronger emission from the SGH-HL survey (e.g., the same X_{CO} applies to both components). However, Liszt and Pety (2012) showed that the CO(1-0) line can be over luminous in diffuse molecular gas. If the newly-detected CO emission arises from this type of gas, then a lower value of X_{CO} would have to be used to determine its contribution to the molecular mass. However, Liszt and Pety (2012) state that in diffuse molecular clouds the lines of sight with $W_{CO} \geq 1.5 \text{ K km s}^{-1}$ are likely to be over luminous. None of the new detections described in this paper are over that threshold. Nevertheless, the issue of what X_{CO} value to use when converting CO(1-0) observations to $\text{N}(\text{H}_2)$ has always been thorny. Further observations, perhaps using the CH line at 3.3 GHz to determine independently $\text{N}(\text{H}_2)$ (e.g., Magnani and Onello 1995), could settle this question.

5 DISCUSSION

By making more sensitive, higher velocity resolution CO(1-0) observations of a region containing a portion of the high-latitude molecular cloud complex, MBM 53-55, we determine that the mass of molecular gas in that region detectable by the CO(1-0) line increases by about a factor of two. If that result is applicable to the entire cloud, then the increase in molecular mass detectable by CO(1-0) observations increases significantly - at the expense of the dark gas estimate for that region. The increase in gas mass comes at the periphery of the cloud and consists of low-surface brightness CO emission. We stress that in addition to greater sensitivity, observations at high velocity resolution (at least 0.1 km s^{-1} per channel) are necessary to detect some of the weak CO emission in diffuse and translucent molecular gas.

Our results are reminiscent of those from mapping the Gemini OB1 molecular cloud complex by Carpenter, Snell, and Schloerb (1995) who find that up to 50% of the CO intensity map may be tied up in low surface brightness gas normally surrounding the dense cores of a GMC. Perhaps we are seeing this phenomenon at lower intensity levels given that we are observing a diffuse/translucent molecular cloud rather than a GMC. In a similar vein, Liszt, Pety, and Lucas (2010) and Goldsmith et al. (2008) have found that a large fraction of CO emission comes from warm (50 - 100 K), low-density ($100 - 500 \text{ cm}^{-3}$), weakly-shielded diffuse molecular gas, even though most of the carbon in these regions is in the form of C^+ .

Low intensity CO emission arising from more diffuse molecular gas than that traced by conventional surveys may be more commonplace in the Galaxy than is currently thought. Dame & Thaddeus (1994) detected a faint, thick molecular disk in the inner Galaxy, with a $12\text{CO}/13\text{CO}$ ratio more similar to that in diffuse and translucent clouds than in GMCs. A similar result has been found by Pety et al. (2013) in M51.

Our results are confined to a small area in the MBM 53-55 cloud complex, but there are other known molecular clouds in the region that were ignored by GCT but detected in the SGH-HL survey. Blair et al. (2017) estimate that these clouds contribute an additional $300 M_{\odot}$ of CO-detectable gas (at typical rms values of 0.1 K). This further reduces

Table 3. Total W_{CO} from the three surveys.

Survey	W_{CO}^a K km s ⁻¹	rms K km s ⁻¹
SGHL-HL survey	7.56	0.93
This paper. SGH-HL detections	8.53	0.37
This paper, new detections	9.89	0.57

^a W_{CO} is defined as $\int T_{mb} dv$

the dark gas inventory in the region from about 40% of the total molecular mass to about 35%. If we assume that sensitive CO observations would also double the mass of these clouds, then the dark gas inventory in the Pegasus Pisces region drops to 30%. This value is similar to what Wolfire, Hollenbach, & McKee (2010) determine on the basis of static PDR models of GMC envelopes. It would appear from our results, that the CO-dark gas fraction does not significantly increase in diffuse and translucent gas. We note that dynamical effects in PDR models could alter the dark gas fraction.

The detection of a significant fraction of CO-dark gas by sensitive CO(1-0) observations is important not just as a proof-of-concept. As mentioned above, spectral line detections also provide velocity information. Moreover, the systematics in using CO data are completely different than those from gamma-ray and infrared observations. CO(1-0) observations are not subject to variations in the gas-to-dust ratio, the uniformity of the cosmic ray environment, or their penetration depth.

We are not advocating that sensitive CO(1-0) observations are the best way to trace dark gas. It is clear that [CII] observations are the best way of spectroscopically tracing this component (see Langer et al. 2010; 2014). However, there have been many claims that as much molecular gas exists in dark as opposed to CO-detectable form (e.g., GCT; Abdo, et al. 2010; Planck Collaboration 2011). In addition, several authors [Barriault et al. (2010); Allen et al. (2012; 2015)], claim the OH 18 cm main lines are better tracers of diffuse molecular gas than the CO(1-0) line. Our results show these claims are premature unless the regions in question have been observed in CO(1-0) both with adequate sensitivity *and* sufficient velocity resolution.

ACKNOWLEDGMENTS

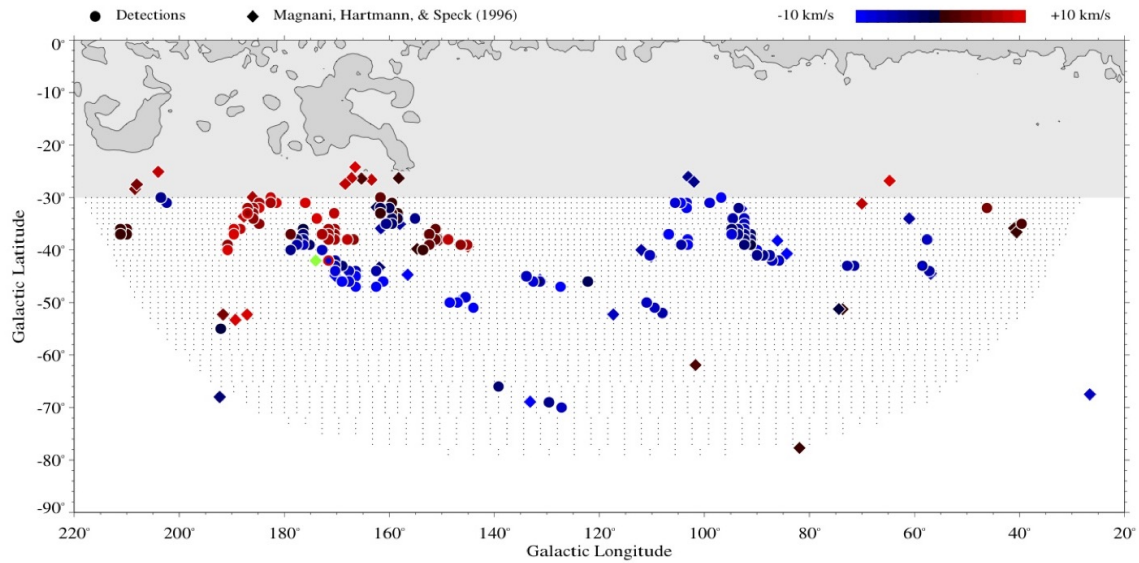
We thank Professor Lucy Ziurys for generously allocating the observing time to complete this project. The Kitt Peak 12 meter radio telescope is operated by the Arizona Radio Observatory (ARO), Steward Observatory, University of Arizona. We also thank Professors Hector Arce and Steven Shore for comments which greatly improved this work. Finally, we thank the anonymous referee who raised several points which clarified and improved the manuscript.

REFERENCES

- Abdo, A.A., et al. 2010, ApJ, 710, 133
 Allen, R.J., Ivette Rodríguez, M., Black, J.H., & Booth, R.S. 2012, AJ, 143, 97

- Allen, R.J., Hogg, D.E., & Engelke, P.D. 2015, AJ, 149, 123
 Barriault, L., Joncas, G., Lockman, F.J., & Martin, P.G. 2010, MNRAS, 407, 2645
 Blair, S., et al. 2017, in preparation
 Carpenter, J.M., Snell, R.L., & Schloerb, F.P. 1995, ApJ, 445, 246
 Chastain, R.J., 2005, Ph.D. Thesis, University of Georgia
 Chastain, R.J., Shelton, R.L., Raley, E.A., & Magnani, L., 2006, AJ, 132, 1964
 Cotten, D.L., Magnani, L., Wennerstrom, E.A., Douglas, K.A., & Onello, J.S. 2012, AJ, 144, 163
 Cotten, D.L. & Magnani, L. 2013, MNRAS, 436, 1152
 Dame, T.M. & Thaddeus, P. 1994, ApJ, 436, L173
 Draine, B.T. 1978, ApJ Suppl, 36, 595
 Goldsmith, P.F., et al. 2008, ApJ, 680, 428
 Grenier, I.A., Casandjian, J.-M., & Terrier, R. 2005, Science, 307, 1292 (GCT)
 Hartmann, D., Magnani, L., and Thaddeus, P. 1998, ApJ, 492, 205
 Hollenbach, D.J. & Tielens, A.G.G.M. 1997, ARAA, 35, 79
 Kutner, M.L. and Ulich, B.L. 1981, ApJ, 250, 341
 Langer, W.D., et al. 2010, A&A, 521, L17
 Langer, W.D., et al. 2014, A&A, 561, 122
 Liszt, H.S. Pety, J., and Lucas, R. 2010, A&A, 518, A45
 Liszt, H.S. & Pety, J. 2012, A&A, 541, A58
 Liszt, H. 2014, ApJ, 783, 17
 Magnani, L., Blitz, L., & Mundy, L. 1985, ApJ, 295, 402
 Magnani, L. & Onello, J.S. 1995, ApJ, 443, 169
 Magnani, L., Hartmann, D., & Speck, B.G. 1996, ApJS, 106, 447
 Magnani, L., Hartmann, D., Holcomb, S.L., Smith, L.E., & Thaddeus, P. 2000, ApJ, 535, 167
 Pety, J., et al. 2013, ApJ, 779, 43
 The Planck Collaboration; Ade, P.A.R., et al. 2011, A&A, 536, A19
 Schlegel, D.J., Finkbeiner, D.P., & Davis, M. 1999, ApJ, 500, 525
 van Dishoeck, E.F. & Black, J.H. 1988, ApJ, 334, 771
 Wolfire, M.G., Hollenbach, D., & McKee, C.F. 2010, ApJ, 716, 1191
 Yamamoto, H., Onishi, T., Mizuno, A., & Fukui, Y. 2003, ApJ, 592, 217 (Y2003)
 Yamamoto, H., Kawamura, A., Tachihara, K., Mizuno, N., Onishi, T., & Fukui, Y. 2006, ApJ, 642, 307

This paper has been typeset from a $\text{\TeX}/\text{\LaTeX}$ file prepared by the author.



sgh_fig1b 5-MAR-1999 20:19 dap hartmann

Figure 1. The Southern Galactic Hemisphere - High Latitude (SGH-HL) CO(1-0) survey. The 4982 grid points which were observed by Magnani et al. (2000) are depicted as the small black dots. Detections from the survey are the round dots color coded in velocity (see top right corner). Other detections from Magnani, Hartmann, and Speck (1996) that were missed by the SGH-HL sampling grid are denoted by diamonds (the green diamond has no velocity information in the literature). The black box denotes the boundary of the region in Pegasus-Pisces included in the GCT dark gas calculations (see text).

(A color version of this figure is available in the online journal.)

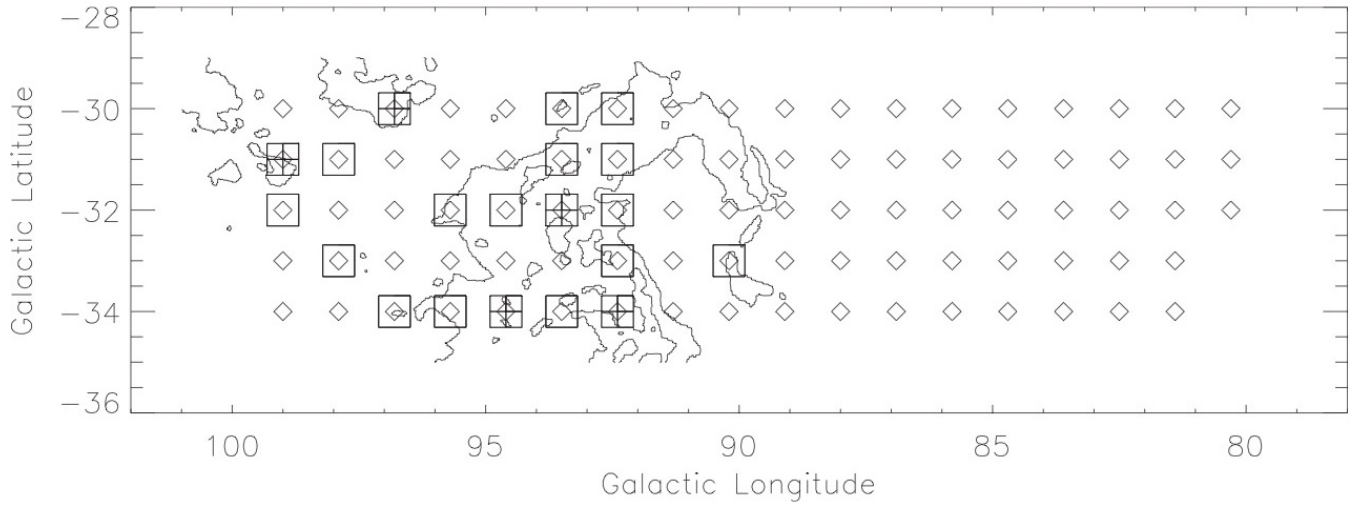


Figure 2. Contour map of the northern portion of MBM 53 in $E(B-V)$ from Schlegel, Finkbeiner, and Davis (1999) in linear scale from 0.10 to 0.51 mag in steps of 0.17 mag. The diamonds indicate the 88 positions that were observed in CO(1-0) for this paper. Each position corresponds to an observation from the SGH-HL survey (see §2). The five CO(1-0) detections from that survey at the T_{mb} level of 0.1 K (listed in Table 1) are denoted by squares with a plus sign in them. The 15 new detections are denoted by squares. Parameters for all the detections are in Table 2.

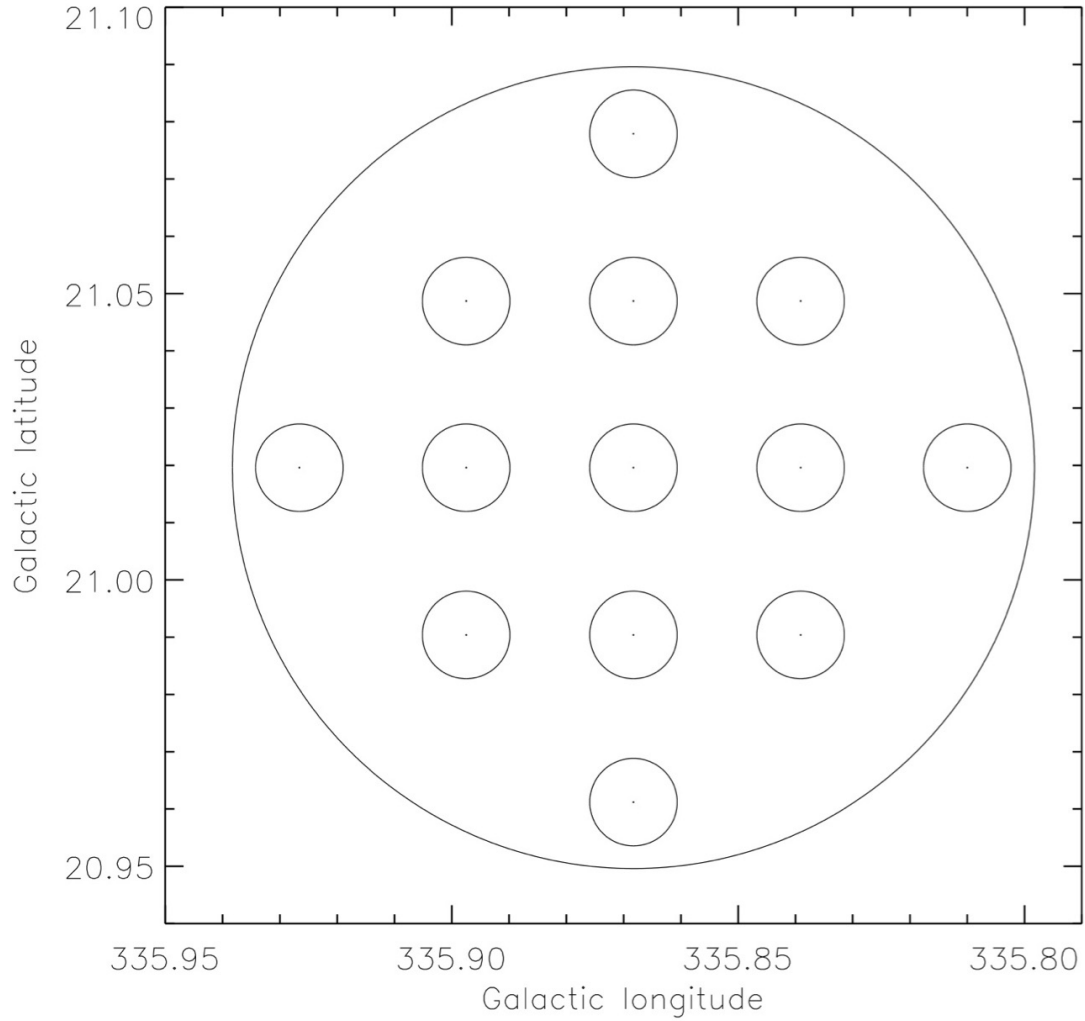


Figure 3. Comparison between the beam of the Harvard Smithsonian – Center for Astrophysics 1.2 m mm-wave telescope (beam size $8.4'$ at 115 GHz) with the 13-point beam pattern from the 12-m Arizona Radio Observatory telescope used to sample the larger beam. The sampling pattern is for one of the 88 observed positions (see Figure 2) and is representative of how each of those positions were observed in CO, with the final spectrum for that position produced by averaging the 13 individual spectra. The beam size of the 12-m at 115 GHz is $55''$.

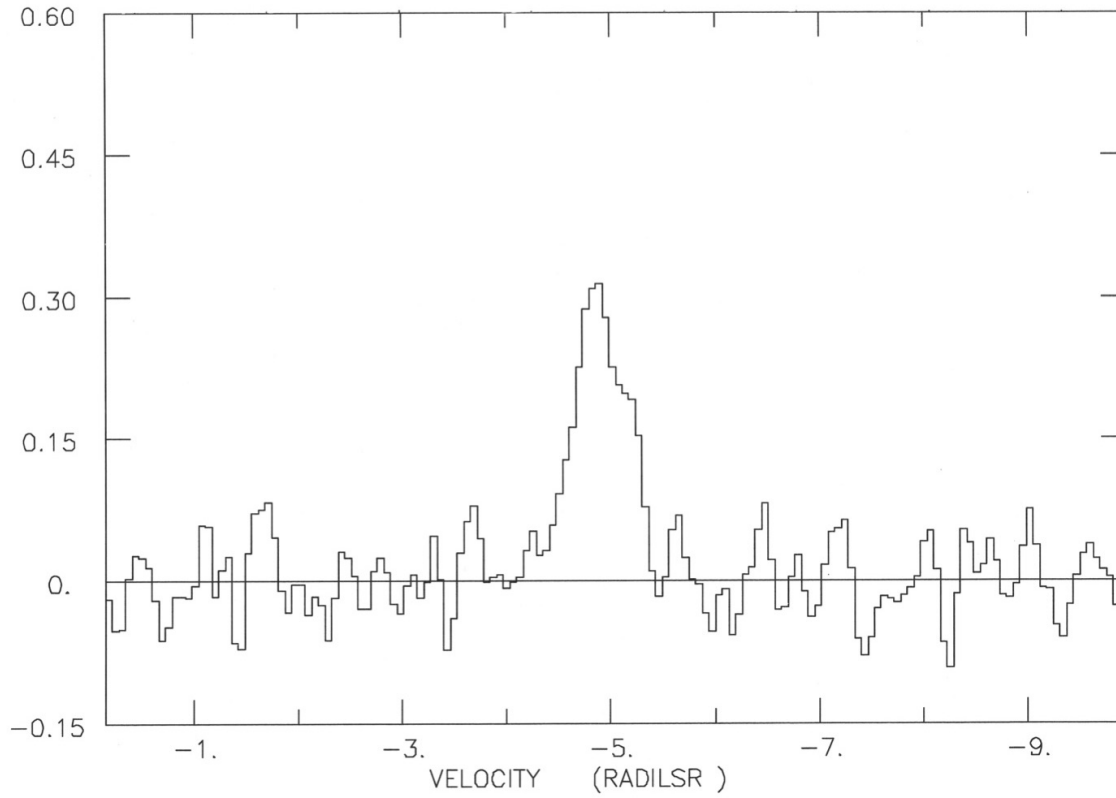


Figure 4a. CO(1-0) spectrum from position $(\ell, b) = (95.7^\circ, -34.0^\circ)$. The y-axis is antenna temperature in K in the form T_R^* and the x-axis denotes v_{LSR} in km s^{-1} . The velocity resolution and rms per channel are 0.06 km s^{-1} and 39 mK, respectively.

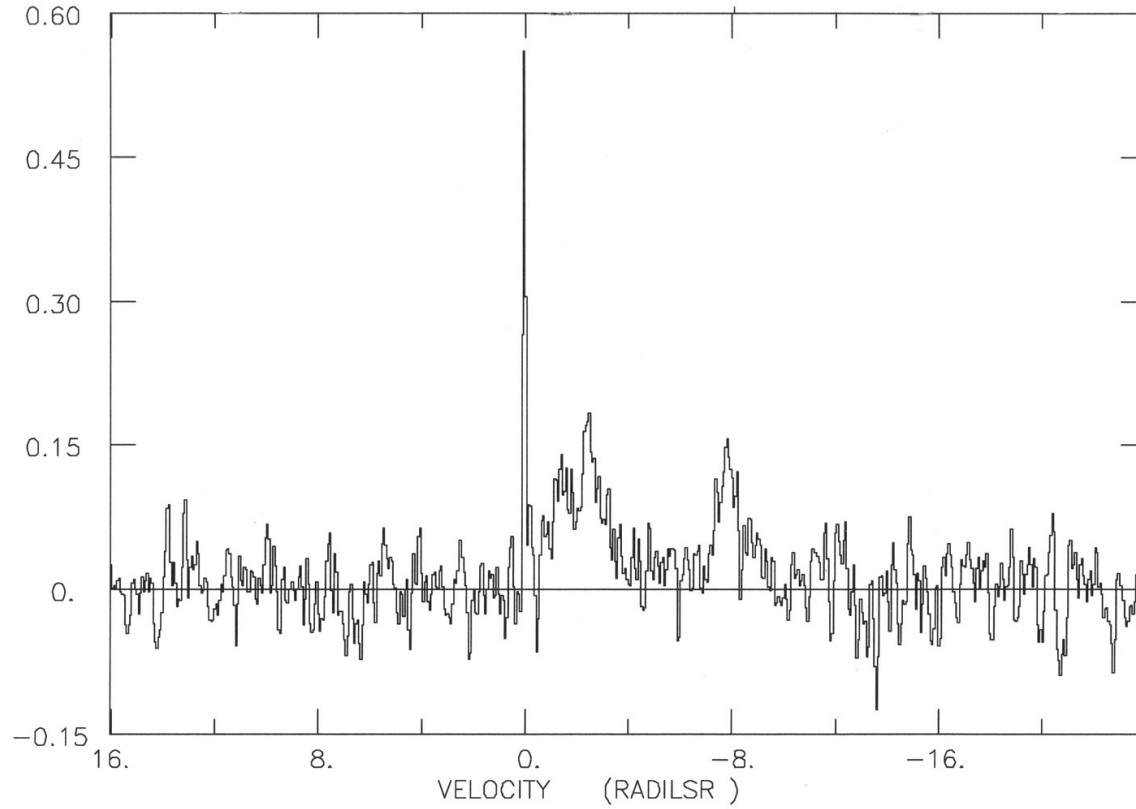


Figure 4b. CO(1-0) spectrum from position $(\ell, b) = (92.4^\circ, -32.0^\circ)$. The x- and y-axes are as in Figure 5a. The rms is 34 mK per channel. The narrow pip at $v_{LSR} \approx 0 \text{ km s}^{-1}$ is RFI from the system electronics.

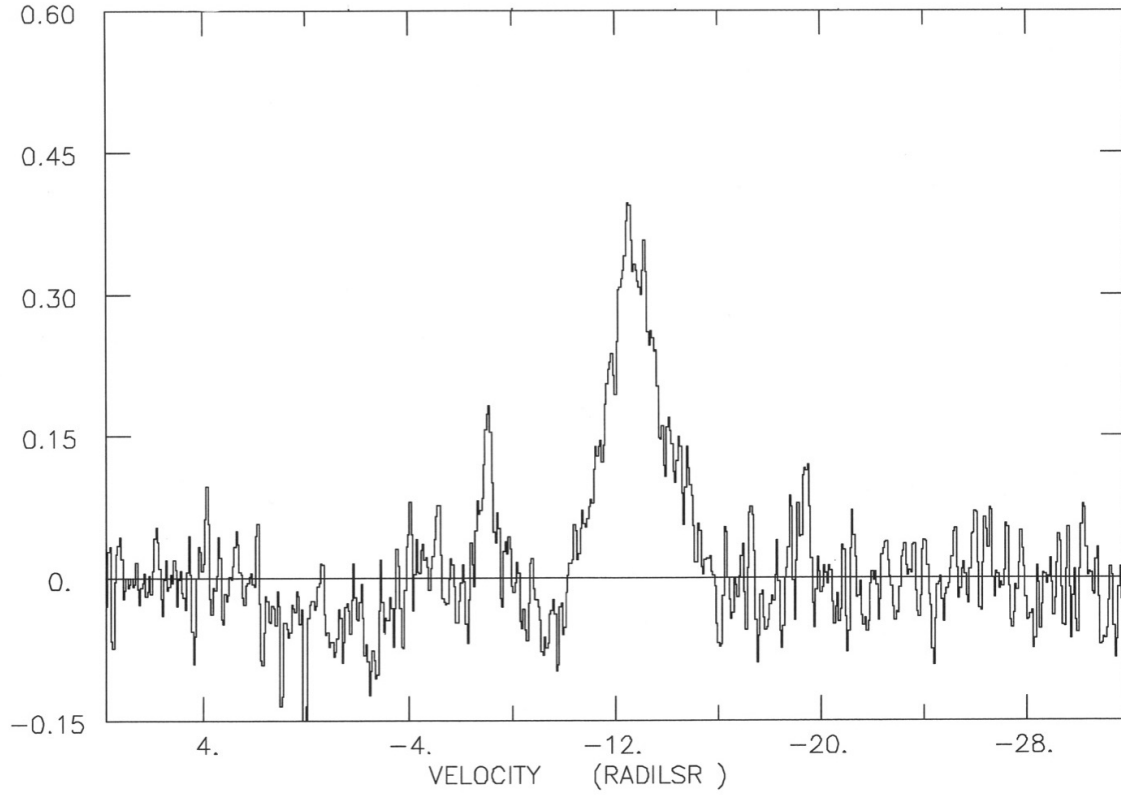


Figure 4c. CO(1-0) spectrum from position $(\ell, b) = (92.4^\circ, -32.0^\circ)$. The The x- and y-axes are as in Figure 5a. The rms is 37 mK per channel.

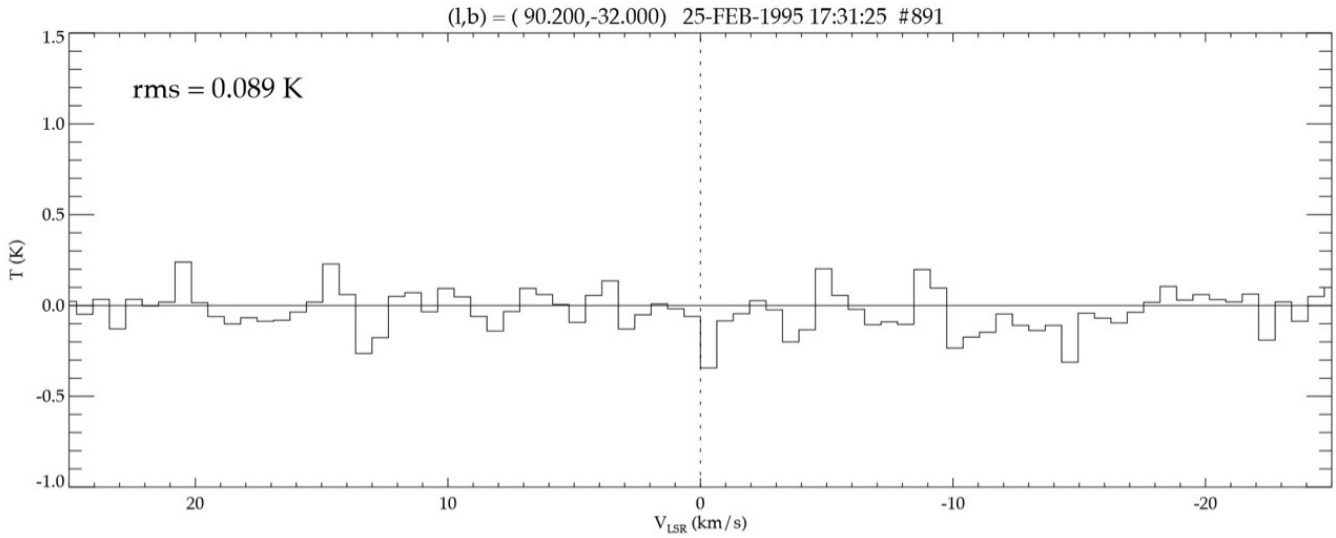


Figure 5a. CO(1-0) spectrum from the SGH-HL survey. The spectrum was made using on-off mode with the on position at $(\ell, b) = (90.2^\circ, -32.0^\circ)$ and the off position at $(\ell, b) = (90.2^\circ, -33.0^\circ)$. See Hartmann, Magnani, and Thaddeus (1998) for details. With this observing technique, if a CO(1-0) emission line were to be present in the off position, it would appear as an absorption line in the spectrum. The y-axis is antenna temperature in K in the form T_R^* . The velocity resolution is 0.65 km s^{-1} .

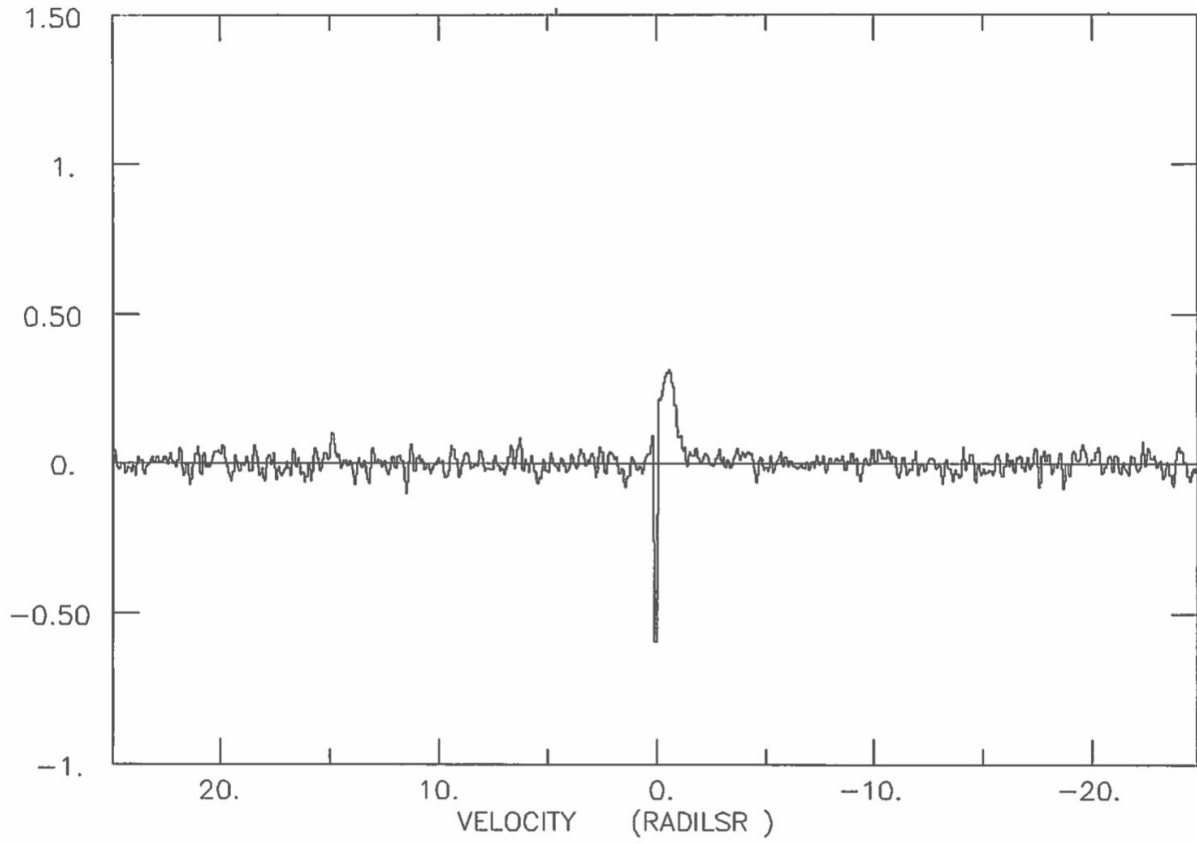


Figure 5b. CO(1-0) spectrum from position $(\ell, b) = (92.4^\circ, -33.0^\circ)$. The FWHM of the line from Gaussian fitting is 0.60 km s^{-1} . The downward going spike at 0 km s^{-1} is interference. The y-axis is antenna temperature in K in the form T_R^* and the x-axis is v_{LSR} in km s^{-1} . The velocity resolution is 0.06 km s^{-1} and the rms is 25 mK.